



The role of asymmetrical and repulsive coupling in the dynamics of two coupled van der Pol oscillators

Sergey Astakhov, Artem Gulai, Naoya Fujiwara, and Jürgen Kurths

Citation: *Chaos* **26**, 023102 (2016); doi: 10.1063/1.4940967

View online: <http://dx.doi.org/10.1063/1.4940967>

View Table of Contents: <http://scitation.aip.org/content/aip/journal/chaos/26/2?ver=pdfcov>

Published by the [AIP Publishing](#)

Articles you may be interested in

[Synchronization of two memristively coupled van der Pol oscillators](#)

Appl. Phys. Lett. **108**, 084105 (2016); 10.1063/1.4942832

[On the stability analysis of a pair of van der Pol oscillators with delayed self-connection, position and velocity couplings](#)

AIP Advances **3**, 112118 (2013); 10.1063/1.4834115

[Transient chaotic rotating waves in a ring of unidirectionally coupled symmetric Bonhoeffer-van der Pol oscillators near a codimension-two bifurcation point](#)

Chaos **22**, 033115 (2012); 10.1063/1.4737430

[Hopf-Bifurcations and Van der Pol Oscillator Models of the Mammalian Cochlea](#)

AIP Conf. Proc. **1403**, 199 (2011); 10.1063/1.3658086

[Bifurcation, amplitude death and oscillation patterns in a system of three coupled van der Pol oscillators with diffusively delayed velocity coupling](#)

Chaos **21**, 023111 (2011); 10.1063/1.3578046



The role of asymmetrical and repulsive coupling in the dynamics of two coupled van der Pol oscillators

Sergey Astakhov,^{1,a)} Artem Gulai,^{2,b)} Naoya Fujiwara,^{3,c)} and Jürgen Kurths^{4,5}

¹Information Security of Automated Systems Department, Yuri Gagarin State Technical University of Saratov, Politekhničeskaya st. 77, Saratov 410054, Russia

²Radioelectronics and Telecommunications Department, Yuri Gagarin State Technical University of Saratov, Politekhničeskaya st. 77, Saratov 410054, Russia

³Center for Spatial Information Science, The University of Tokyo, 277-8568 Chiba, Japan

⁴Potsdam Institute for Climate Impact Research (PIK), 14473 Potsdam, Germany

⁵Institute for Complex Systems and Mathematical Biology, University of Aberdeen, Aberdeen, United Kingdom

(Received 17 October 2015; accepted 14 January 2016; published online 28 January 2016)

A system of two asymmetrically coupled van der Pol oscillators has been studied. We show that the introduction of a small asymmetry in coupling leads to the appearance of a “wideband synchronization channel” in the bifurcational structure of the parameter space. An increase of asymmetry and transition to repulsive interaction leads to the formation of multistability. As the result, the tip of the Arnold’s tongue widens due to the formation of folds defined by saddle-node bifurcation curves for the limit cycles on the torus. © 2016 AIP Publishing LLC.

[<http://dx.doi.org/10.1063/1.4940967>]

One of the basic models of self-oscillating systems is the van der Pol oscillator. This model is widely used in studies of synchronization phenomena of quasi-harmonic periodic oscillations. The bifurcation mechanisms underlying the mutual synchronization of two van der Pol oscillators can be described comprehensively by the well-known structure called the Arnold tongue on the parameter plane spanned by natural frequency mismatch and coupling coefficient. The distinguishing feature of this structure is that the bifurcation curves limiting the synchronization region converge to a single point when a coupling parameter decreases. At zero value of the coupling coefficient, synchronization disappears. In this paper, we show that transition to an asymmetrical and repulsive coupling leads to substantial changes in bifurcation structure of the Arnold tongue, particularly to an expansion of synchronization region at small coupling coefficient values, to disappearance of the tip of Arnold tongue, and to the formation of a multistability region.

I. INTRODUCTION

Synchronization phenomena are very important for science and technology and have attracted high attention among researchers in different fields of science.^{1,2} Synchronization can be observed in systems of different nature and complexity.^{3–9} Besides, synchronization can be realized for different types of oscillations: periodic,¹⁰ quasi-periodic,^{11–13} chaotic,^{14–17} and stochastic.^{2,8,18,19}

Usually, when synchronization of a specific type of oscillations is studied, one uses paradigmatic models which, on the one hand, demonstrate some wanted behavior, and on

the other hand these models have a rather simple form and can be described by, e.g., a rather simple system of differential equations. One of the basic models for a periodic self-sustained oscillator is the van der Pol oscillator,²⁰ which has been widely used for the study of mutual and external synchronization phenomena in small and large ensembles with different types and topologies of coupling.^{21,22}

It should be noted that it is the type of coupling which defines essential peculiarities of the behavior of interacting oscillators, particularly van der Pol oscillators. In Ref. 23, it has been shown that the character of the coupling defines the stability of a specific dynamical regime as well as the formation of multistability in a system of two interacting van der Pol oscillators.

Recently, the attention of researchers has been attracted to asymmetrical coupling²⁴ and repulsive coupling.^{25,26} In particular, these types of coupling have become popular due to the recent successes in synthetic biology, where coupling is realized naturally in a system of genetic oscillators (repressors).²⁷ Moreover, the asymmetrical and repulsive interaction is typical for other biological systems, e.g., neural ensembles and networks. It is well known that such biological networks incorporate different types of interaction due to the existence of excitatory and inhibitory synapses in the brain, which enhance synchronization and signal transmission.²⁸ The different types of interaction introduce asymmetry which can be quantitatively realized in different phase shifting leading to various special effects. In Ref. 29, pattern formation has been studied in a two-dimensional array of oscillators with a phase-shifting interaction. Particularly, the phase shift of π which corresponds to the repulsive interaction was considered there. The repulsive interaction also attracted author’s attention in Ref. 30 where the effect of the network topology on the dynamics of non-identical oscillators has been studied. It has been shown that a small amount of repulsive connections increases activity and

^{a)}Electronic mail: s.v.astakhov@gmail.com

^{b)}Electronic mail: gulai.artem@gmail.com

^{c)}Electronic mail: fujiwara@csis.u-tokyo.ac.jp

synchronization in the whole network. The existence of nodes with repulsive links facilitates the propagation of activity in a network. It also should be noted that the repulsive coupling is presented not only in biological systems, e.g., in Ref. 31, a chain of repulsively coupled chaotic oscillators has been studied and compared with an experimental laser system with negative feedback and delay.

The role asymmetrical and repulsive coupling plays in synchronization of two van der Pol oscillators by external harmonic forces has been considered in Ref. 32 with the help of phase-reduction approach. It has been shown that the structure of the phase space of the Kuramoto phase oscillators becomes substantially more complicated when an asymmetrical repulsive coupling is introduced. In the system of phase oscillators, besides the saddle-node bifurcations, the Andronov-Hopf bifurcations can be realized which leads to multistability in this system. However, a detailed analysis of the non-reduced system of van der Pol oscillators has not been done yet. Moreover, a detailed bifurcation analysis of an autonomous system of two van der Pol oscillators with an asymmetrical repulsive coupling has not been done is also an open problem.

Therefore, we study here the dynamics of an autonomous system consisting of two van der Pol oscillators with asymmetrical repulsive coupling and carry out a bifurcation analysis for both the amplitude-phase reduced model (Stuart-Landau equations) and the non-reduced initial model. We suppose that such two-way consideration is important because the use of amplitude-phase reduction decreases the phase space dimension and simplifies the analysis of its structure and bifurcations. Moreover, the Stuart-Landau model is frequently used as an independent one.³³

This paper is organized as follows. In Sec. II, we derive and analyze the dynamics and bifurcations in a reduced model of two asymmetrically coupled van der Pol oscillators. In Sec. III, we analyze the non-reduced system and compare it with the results obtained in Sec. II. In Conclusions, we summarize the presented results and discuss their possible application.

II. QUASIHARMONIC APPROACH

A. Derivation of the system equations

A system of two van der Pol oscillators with an asymmetrical repulsive coupling can be written in the following form:

$$\begin{cases} \ddot{x}_1 - (\varepsilon - x_1^2)\dot{x}_1 + \omega_1^2 x_1 - \gamma_1(\dot{x}_2 - \dot{x}_1) = 0, \\ \ddot{x}_2 - (\varepsilon - x_2^2)\dot{x}_2 + \omega_2^2 x_2 - \gamma_2(\dot{x}_1 - \dot{x}_2) = 0. \end{cases} \quad (1)$$

Here, $x_{1,2}$ are the dynamical variables of the first and second oscillators, respectively, ε is a control parameter which characterizes the linear dissipation in the system, $\omega_{1,2}$ are the natural frequencies of the first and second oscillators, respectively, and $\gamma_{1,2}$ are the coupling coefficients where $\gamma_1 \neq \gamma_2$ in the general case.

According to the quasiharmonic approach, we find the following solution for Eq. (1):³⁴

$$\begin{aligned} x_{1,2}(t) &= \frac{A_{1,2}(t)e^{j\omega t}}{2} + \frac{A_{1,2}^*(t)e^{-j\omega t}}{2}, \\ \dot{x}_{1,2} &= \frac{1}{2} \left(A_{1,2}j\omega e^{j\omega t} - A_{1,2}^*j\omega e^{-j\omega t} \right), \end{aligned}$$

where ω is some frequency which is common for both interacting oscillators in the regime of synchronization. Then, the variables $A_{1,2}$ have to satisfy the following condition:

$$\dot{A}_{1,2}e^{j\omega t} + \dot{A}_{1,2}^*e^{-j\omega t} = 0,$$

and the second derivatives are

$$\ddot{x}_{1,2} = \dot{A}_{1,2}j\omega e^{j\omega t} - \frac{1}{2} \left(A_{1,2}\omega^2 e^{j\omega t} + A_{1,2}^*\omega^2 e^{-j\omega t} \right).$$

Sequential substitution of the obtained derivatives, divide by $j\omega e^{j\omega t}$, and averaging over the period $\frac{2\pi}{\omega}$ gives the following:

$$\begin{cases} \dot{A}_1 - \frac{\varepsilon A_1}{2} + \frac{1}{8}|A_1|^2 A_1 + j\frac{\omega^2 - \omega_1^2}{2\omega} A_1 + \frac{\gamma_1}{2}(A_1 - A_2) = 0, \\ \dot{A}_2 - \frac{\varepsilon A_2}{2} + \frac{1}{8}|A_2|^2 A_2 + j\frac{\omega^2 - \omega_2^2}{2\omega} A_2 + \frac{\gamma_1}{2}(A_2 - A_1) = 0. \end{cases} \quad (2)$$

We denote $\frac{\omega^2 - \omega_{1,2}^2}{2\omega} = \Delta_{1,2}$, $\frac{\gamma_{1,2}}{2} = g_{1,2}$ and rewrite the complex amplitudes as

$$A_{1,2} = \rho_{1,2} e^{j\varphi_{1,2}}. \quad (3)$$

As a result, we get the following system of equations:

$$\begin{cases} \dot{\rho}_1 + j\dot{\varphi}_1 \rho_1 - \frac{\varepsilon}{2}\rho_1 + \frac{1}{8}\rho_1^3 + j\Delta_1 \rho_1 + g_1 \rho_1 - g_1 \rho_2 e^{j(\varphi_2 - \varphi_1)} = 0, \\ \dot{\rho}_2 + j\dot{\varphi}_2 \rho_2 - \frac{\varepsilon}{2}\rho_2 + \frac{1}{8}\rho_2^3 + j\Delta_2 \rho_2 + g_2 \rho_2 - g_2 \rho_1 e^{j(\varphi_1 - \varphi_2)} = 0. \end{cases} \quad (4)$$

Next, we introduce the phase difference variable $\phi = \varphi_2 - \varphi_1$ and denote the parameter mismatches $\delta = \Delta_1 - \Delta_2$, $g = g_1$, $\Delta_g = g_2 - g_1$. Separating the real part from the imaginary part in Eq. (4), one obtains

$$\begin{cases} \dot{\rho}_1 = \frac{\varepsilon}{2}\rho_1 - \frac{1}{8}\rho_1^3 + g(\rho_2 \cos(\phi) - \rho_1), \\ \dot{\rho}_2 = \frac{\varepsilon}{2}\rho_2 - \frac{1}{8}\rho_2^3 + (g + \Delta_g)(\rho_1 \cos(\phi) - \rho_2), \\ \dot{\phi} = \delta - \left((g + \Delta_g) \frac{\rho_1}{\rho_2} + g \frac{\rho_2}{\rho_1} \right) \sin(\phi). \end{cases} \quad (5)$$

We should note that the obtained system is three-dimensional and the axis corresponding to the variable ϕ is 2π -periodic.

B. Bifurcational analysis of the reduced system

Now we analyze changes in the phase space structure and bifurcations in (5) versus the variation of control parameters. We first fix the following values of control parameters: $\varepsilon = 0.25$, $\delta = 0.01$, $g = 0.045$, and $\Delta_g = 0$.

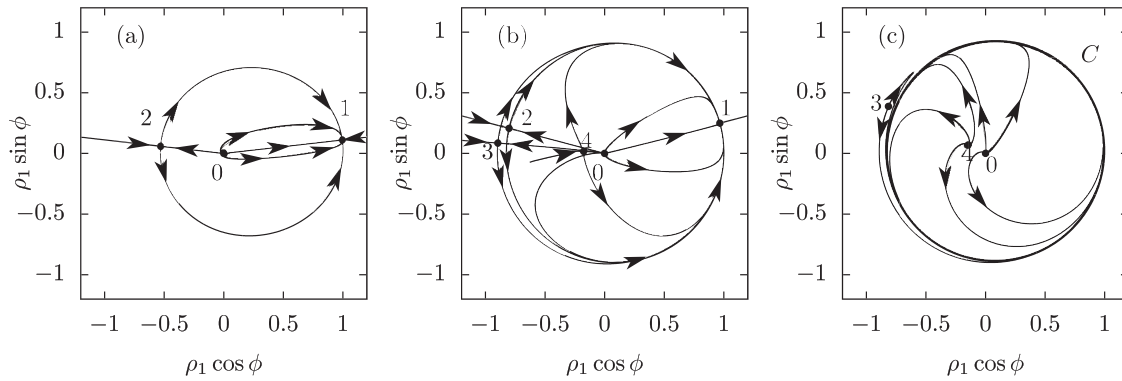


FIG. 1. The projections of the phase portraits of system (5) on $(\rho_1 \cos \phi, \rho_1 \sin \phi)$ plane with $\varepsilon = 0.25$, $\delta = 0.01$, $\Delta_g = 0$ and (a) $g = 0.045$; (b) $g = 0.02$; and (c) $g = 0.0025$. Here, 1 is a stable node; 2, 3, 4 are saddles; 0 is a repeller; and C is a stable limit cycle. It should be noted that the crossing of curves observed in panel (b) is the result of projection of the 4-dimensional phase space on a plane, and it does not correspond to an intersection of the phase trajectories.

The corresponding phase portrait is represented in Fig. 1(a). The observed structure remains in a certain interval of the natural frequency mismatch δ . Now fix $\delta = 0.01$ and follow the bifurcational transitions in (5) versus the coupling coefficient g . The corresponding bifurcation diagram is represented in Fig. 2(a). It is clearly seen that decreasing of the coupling coefficient leads to the sequential emergence of a pitchfork bifurcation (P_3) and a saddle-node bifurcation (SN). The pitchfork bifurcation leads to the emergence of new saddle equilibrium states (denoted by 3 and 4), which are shown in Fig. 1(b). The stable equilibrium state undergoes a saddle-node bifurcation when the value of the mismatch parameter δ is varied. The corresponding bifurcation diagram is represented in Fig. 2(b). In Fig. 3(a), we show a two-parametric bifurcation diagram on the (δ, g) plane. This diagram represents the well-known structure of a synchronization (Arnold) tongue which was described in, e.g., Ref. 23. Here, region I corresponds to the situation when the system has only one attractor which is a stable equilibrium point in the origin. Regions II, III, IV correspond to a stable equilibrium with non-zero coordinates. Region V corresponds to a stable limit cycle. The curves $l_{P_{1,2,3}}$ denote pitchfork bifurcations, l_{AH} and l_{SN} denote Andronov-Hopf and saddle-node bifurcations, respectively.

Now we evaluate the role which the asymmetry plays which is introduced into the coupling channel by setting the value $\Delta_g = -0.005$. For this case, a bifurcation diagram on

the parametric plane (δ, g) is represented in Fig. 3(b). By comparing the structures of the synchronization regions in Figs. 3(a) and 3(b), one can see some changes induced by the asymmetry in the coupling. There two curves replace a single curve separating regions I and V in the case of symmetrical coupling: l_{P_2} and l_{AH} . Therefore, a channel appeared which is confined by these two new curves. This channel enables us to observe a phase space structure which is equivalent to the case of $\delta = 0$ even for significant values of frequency mismatch δ . The emergence of this channel and its structure were studied in, e.g., Refs. 35 and 36. It was shown there that a necessary condition for the emergence of this channel was the nonidentity of the interacting systems in their nonlinearity parameters. In contrast, here the nonidentity is provided by the coupling asymmetry (see Eq. (5)).

Now we increase the asymmetry in interaction by setting $\Delta_g = -0.05$. The corresponding bifurcation diagram is shown in Fig. 3(c). The main difference in the bifurcational structure from the cases considered above is the emergence of a widened region on the tip of synchronization tongue for small values of the g . Let us consider this region in more detail (see Fig. 3(d)). It can be seen that there is an overlaying of two regions limited with different saddle-node bifurcation curves. Therefore, by varying the value of δ at small values of g , there occur two saddle-node bifurcations which lead to the emergence of two stable equilibrium states. Thus, we show for small values of g and for a small mismatch parameter δ system (5) is characterized by bistability. There

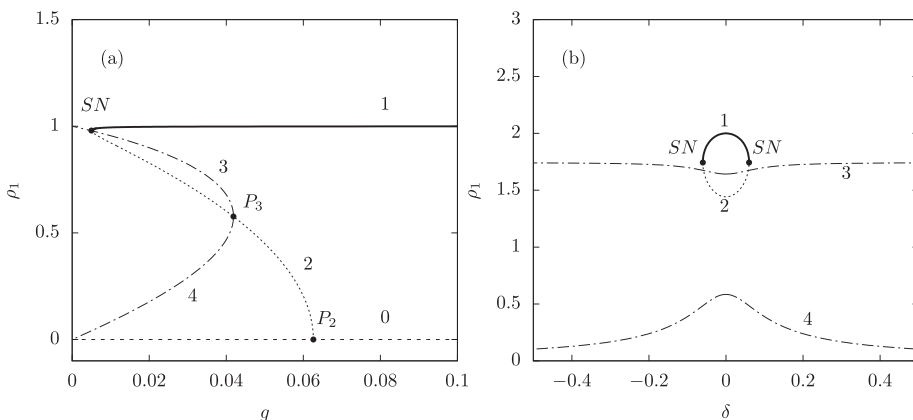


FIG. 2. Bifurcation diagrams of system (5): (a) $\varepsilon = 0.25$, $\delta = 0.01$, $\Delta_g = 0$ and (b) $\varepsilon = 0.25$, $g = 0.03$, $\Delta_g = 0$. Here, 1 is a stable node; 2, 3, 4 are saddles; 0 is an unstable node (repeller); SN is the point of saddle-node bifurcation; and $P_{2,3}$ are points of pitchfork bifurcation. Solid and dashed lines represent stable and unstable fixed points, respectively.

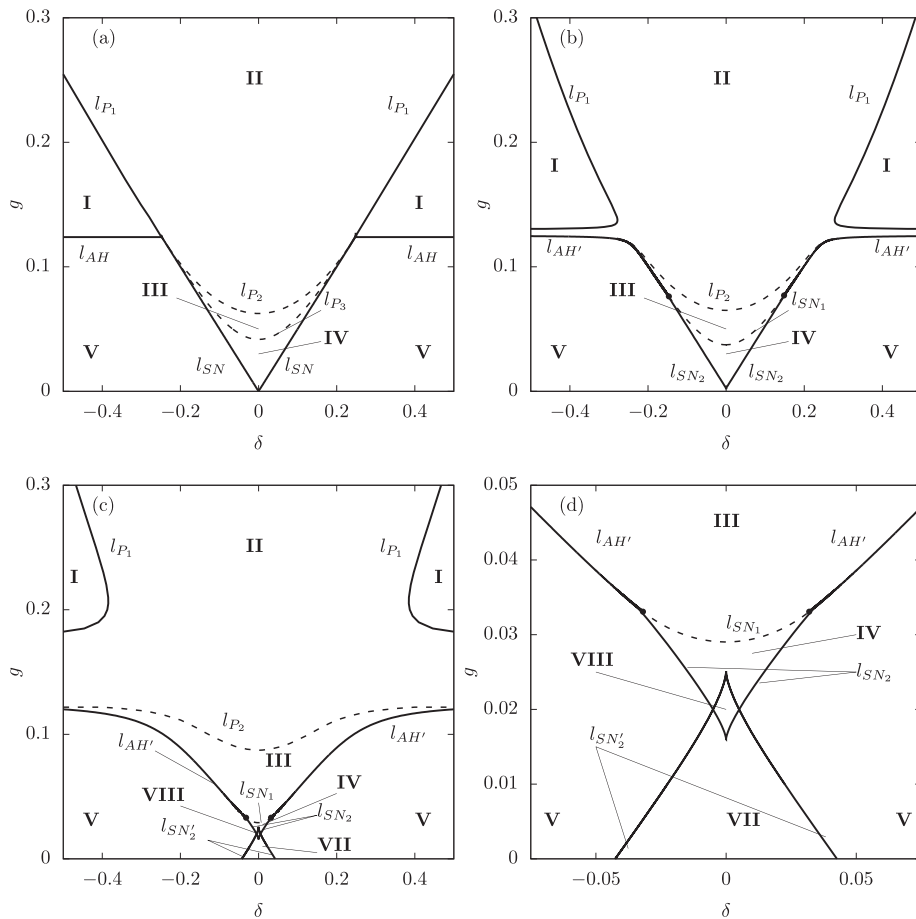


FIG. 3. Bifurcation diagram for the reduced system (5): (a) $\Delta_g = 0$; (b) $\Delta_g = -0.005$; and (c) and (d) $\Delta_g = -0.05$. Region near $\delta = 0$ in (c) is enlarged in panel (d). Region I corresponds to a stable equilibrium point in the origin; regions II, III, IV correspond to a stable equilibrium with non-zero coordinates; and region V corresponds to a stable limit cycle. The curves $l_{P_{1,2,3}}$ denote pitchfork bifurcations, l_{AH} and l_{SN} denote Andronov-Hopf and saddle-node bifurcations, respectively.

are two stable equilibrium states in the phase space on the same closed invariant curve, which are separated by two saddle equilibrium points (see Fig. 4).

Based on the presented bifurcational analysis of the reduced model (5), one can expect that the bistability can be expected in the initial system of two asymmetrically coupled van der Pol oscillators (1). Since the fixed points in the

reduced equation correspond to limit cycles in the original system, one should expect the emergence of two stable limit cycles situated on the surface of a single two-dimensional torus for small values of the coupling coefficient and the mismatch in the natural frequencies.

III. NON-REDUCED SYSTEM

A. Symmetrical coupling

Now we analyze the dynamics of the non-reduced system of two symmetrically coupled van der Pol oscillators denoted by Eq. (1). It should be noted that a similar analysis was carried out earlier (see Ref. 36). We recall these results in order to use them in our studies. Before we start the bifurcational analysis, it is convenient to rewrite the initial system (1) in the following form:

$$\begin{cases} \ddot{x}_1 - (\varepsilon - x_1^2)\dot{x}_1 + x_1 = \gamma(\dot{x}_2 - \dot{x}_1), \\ \ddot{x}_2 - (\varepsilon - x_2^2)\dot{x}_2 + p^2x_2 = (\gamma + \Delta_\gamma)(\dot{x}_1 - \dot{x}_2). \end{cases} \quad (6)$$

Here, we set $\omega_1 = 1$ and denote $p = \omega_2/\omega_1$, $\gamma = \gamma_1$, $\Delta_\gamma = \gamma_2 - \gamma_1$, the rest parameters and variables are the same as in Eq. (1). At first, we consider the dynamics of system (6) in case of symmetric coupling with $\Delta_\gamma = 0$, while the nonlinearity parameter ε is increasing and the other parameters are fixed at the following values: $\gamma = 0.15$ and $p = 1.1$. The corresponding bifurcation diagram is represented in Fig. 5(a). As one can see, the only attractor for $\varepsilon < 0$ is an equilibrium state. At $\varepsilon = 0.0381$, the equilibrium state undergoes

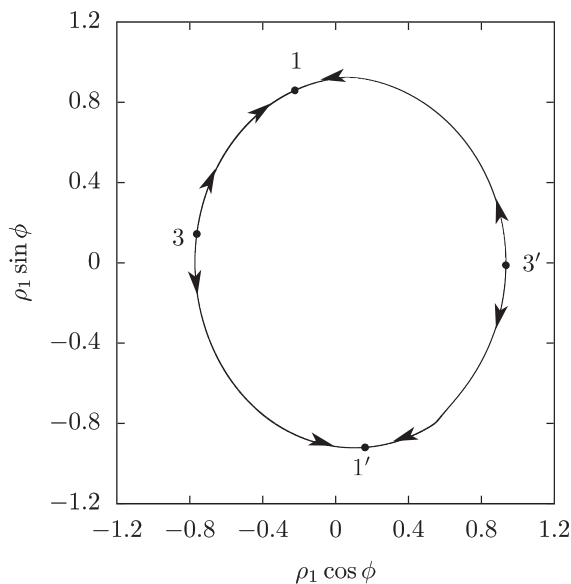


FIG. 4. Phase portrait of system (5) with $\Delta_g = -0.05$, $\varepsilon = 0.25$, $\delta = 0.002$, $g = 0.02$.

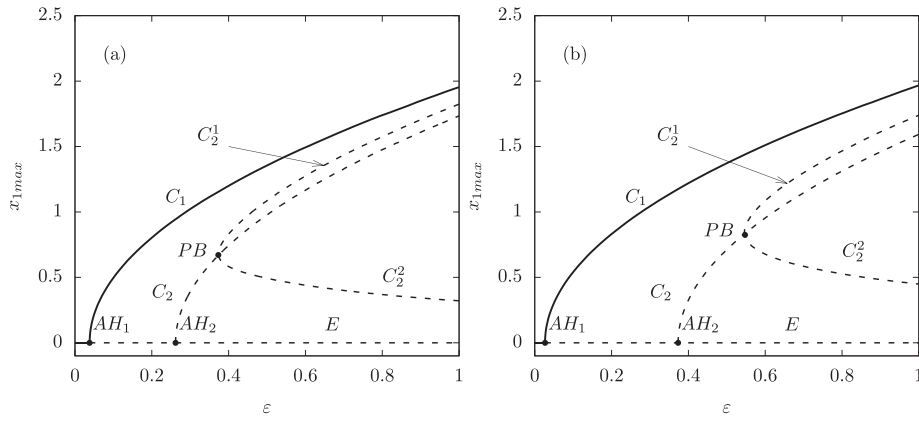


FIG. 5. Bifurcation diagram for system (6) with $p = 1.1$, $\varepsilon \in [0, 1]$ and (a) $\gamma = 0.15$; (b) $\gamma = 0.2$. Here, $AH_{1,2}$ are the Andronov-Hopf bifurcations, PB is the pitchfork bifurcation, E is the equilibrium state, and $C_{1,2}$ and $C_{2,2}^{1,2}$ are the limit cycles.

an Andronov-Hopf bifurcation AH_1 and a steady limit cycle C_1 appears. Further increase of ε leads to a second Andronov-Hopf bifurcation AH_2 of the fixed point (which is a saddle before this bifurcation), resulting into the appearance of a saddle limit cycle C_2 . The relative position of these limit cycles is represented in Figs. 6(a) and 6(b). At larger values of ε , the saddle limit cycle C_2 undergoes a pitchfork bifurcation (denoted PB in Figure 5). After this bifurcation, three unstable limit cycles (C_2 , C_2^1 , and C_2^2) appear in the phase space besides the stable limit cycle C_1 (see Figs. 6(c) and 6(d)). Variation of the coupling coefficient γ leads to a shifting of the bifurcational values of the control parameters. The bifurcation diagram for $\gamma = 0.2$ is depicted in Fig. 5(b). It can be easily seen that the bifurcations are now shifted to the right along the parametric axis.

The influence of the coupling parameter has been studied with a two-parametric bifurcation analysis. The corresponding bifurcation diagram on the parametric plane (ε, γ) is represented in Fig. 7(a). There are five regions which can be distinguished in the diagram. In region I, the dynamical system (6) is characterized by an attractor E which is focus. Region I is limited by two bifurcational curves on its right side: l_{AH_1} and l_T . The curve l_{AH_1} corresponds to an Andronov-Hopf bifurcation of the fixed point E . Therefore, in region II, system (6) demonstrates a stable limit cycle and the saddle fixed point E . The right side of region II is limited with another curve l_{AH_2} for an Andronov-Hopf bifurcation of the saddle equilibrium state E . The saddle limit cycle C_2 appears in the phase space as the result of this bifurcation. Hence, in the range of the control parameters in region III,

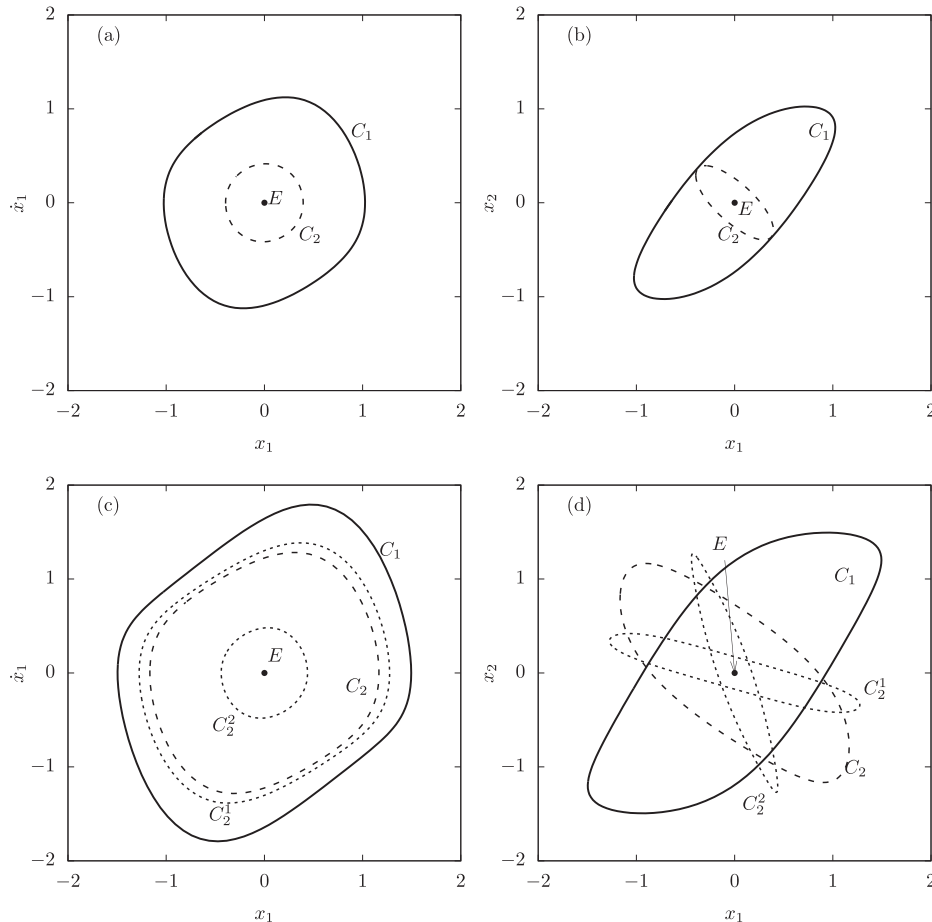


FIG. 6. Phase portraits of the limit cycles in system (6) with $p = 1.1$, $\gamma = 0.15$ and (a), (b) $\varepsilon = 0.3$; (c), (d) $\varepsilon = 0.5$.

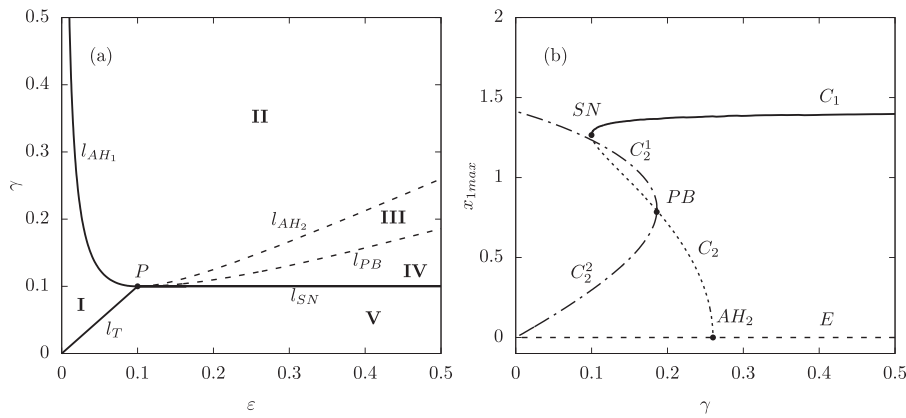


FIG. 7. (a) Two-parametric bifurcation diagram for system (6) on the parametric plane (ϵ, γ) for $p = 1.1$. Here, $l_{AH_{1,2}}$ are the Andronov-Hopf bifurcation curves, l_{PB} is the pitchfork bifurcation curve, and l_{SN} is the saddle-node bifurcation curve. (b) Bifurcation diagram for system (6) for $p = 1.1$, $\epsilon = 0.5$, $\gamma \in [0, 0.5]$. Here, E is the fixed point, C_1 is the stable limit cycle, C_2 , C_2^1 , and C_2^2 are the unstable limit cycles, AH_2 is the Andronov-Hopf bifurcation, PB is the pitchfork bifurcation, and SN is the saddle-node bifurcation.

the phase space includes two limit cycles (the stable one and the saddle one) and the unstable fixed point E . One can see their relative position in Figs. 6(a) and 6(b). Region III is limited by the pitchfork bifurcation curve l_{PB} at bottom. This bifurcation occurs with the saddle limit cycle C_2 . In region IV, the system is characterized by the unstable fixed point E and four limit cycles: the stable cycle C_1 and three unstable cycles C_2 , C_2^1 , and C_2^2 . Regions IV and V are separated by the saddle-node bifurcation curve for the limit cycles C_1 and C_2 . These cycles are situated on the surface of a two-dimensional torus, and after a tangency bifurcation the torus becomes the only attractor in system (6). Regions I and V are separated by the bifurcation curve l_T . This bifurcation

corresponds to the birth of a stable two-dimensional torus in the vicinity of the equilibrium state E . This bifurcation is degenerate. Further, we show that this degeneracy can be avoided by introducing asymmetry into system (6). The bifurcation diagram presented in Fig. 7(b) illustrates the transition from region II to region V.

Now we fix the control parameter $\epsilon = 0.15$ which corresponds to the only limit cycle C_1 in the phase space. Varying the coupling coefficient γ and the natural frequency mismatch parameter p , one can observe synchronization phenomena in two coupled van der Pol oscillators (6). These phenomena are described in the bifurcation diagram in Fig. 8(a). We find there synchronization as well as amplitude

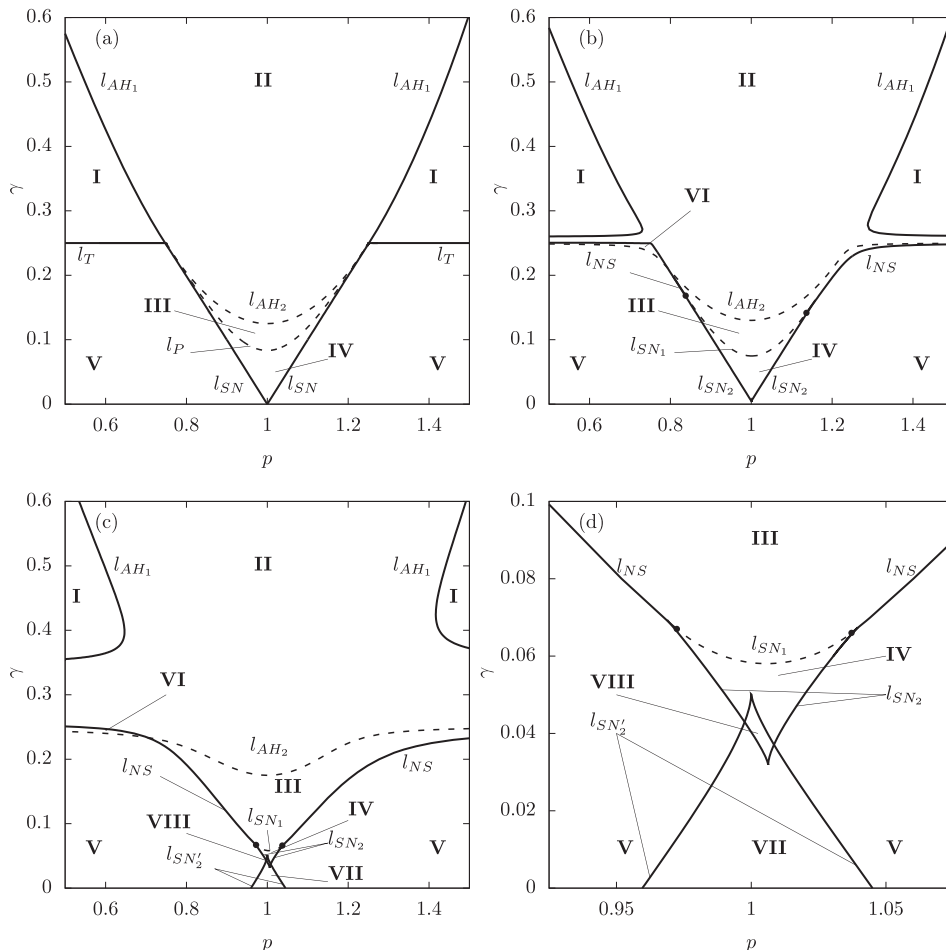


FIG. 8. Bifurcation diagram for system (6) on the parametric plane (p, γ) : (a) $\Delta_\gamma = 0$; (b) $\Delta_\gamma = -0.01$; and (c) and (d) $\Delta_\gamma = -0.1$. Here, $p = \omega_1/\omega_2$, $\omega_1 = 1$, and $\epsilon = 0.15$; $l_{AH_{1,2}}$ are curves for the Andronov-Hopf bifurcations; l_{PB} is the pitchfork bifurcation curve; and l_{SN} is the curve for the saddle-node bifurcation.

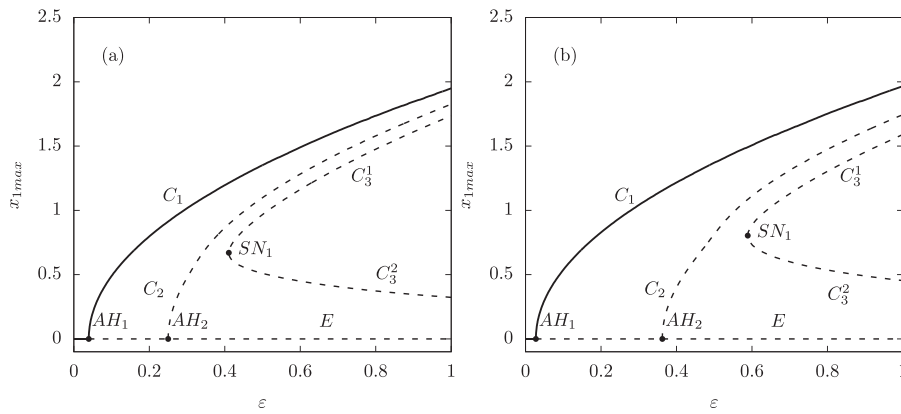


FIG. 9. Bifurcation diagram for system (6) with $p = 1.1$, $\varepsilon \in [0, 1]$, $\Delta_\gamma = -0.01$ and (a) $\gamma = 0.15$; (b) $\gamma = 0.2$. Here, $AH_{1,2}$ are the Andronov-Hopf bifurcations, E is the equilibrium state, and $C_{1,2}$ and $C_3^{1,2,3}$ are the limit cycles.

death. It should be noted that the results obtained for the non-reduced system (6) in case of symmetrical coupling completely correspond to the results obtained for the reduced model (5) by taking into account the increase of phase space dimension.

It should be also noted that the presented results are well known and became a part of classical synchronization theory. However, it is necessary to recall these results before new phenomena for the asymmetrical case, which are presented below will be described from the viewpoint of this theory.

B. The role of asymmetry

Now we consider the influence of asymmetry in the coupling of two interacting oscillators on the bifurcational structures, in particular, the emergence of oscillations and their synchronization. In order to do this, we set $\Delta_\gamma \neq 0$ in (6). Let us consider the evolution of the bifurcation diagram in Fig. 5 induced by varying of Δ_γ . In Fig. 9(a), one can see that asymmetry avoids the degeneracy and the pitchfork bifurcation is replaced by a saddle-node bifurcation. Also, the parameter values corresponding to the Andronov-Hopf bifurcations shift when the asymmetry is introduced into the coupling.

By comparing the results presented in Figs. 7(a) and 10, we see that the introduction of asymmetry in the coupling leads to a splitting of the curve l_T into three bifurcation curves: l_{AH_1} , l_{AH_2} , and l_{NS} . Now the transition from region I to region V leads to three consequent bifurcations: the first Andronov-Hopf bifurcation of the fixed point E leading to the emergence of the stable limit cycle C_1 , the second Andronov-Hopf bifurcation of E and the Neimark-Sacker bifurcation of the limit cycle C_1 . Also, we should note that there appears a region in the parametric plane where the asymmetry induces the stable periodic oscillating regime C_1 , while for $\Delta_\gamma = 0$ the system demonstrates only the equilibrium E .

The asymmetry affects not only the emergence of self-sustained oscillations but also synchronization of interacting oscillators. Varying Δ_γ , one can observe changes in bifurcational structures in the parametric plane (p, γ) (Fig. 8(b)). The mismatch in the coupling parameter leads to the same consequences as in the case of nonequality in the nonlinearity parameter ε for interacting systems:^{35,36} the curves

separating the amplitude death region and the region for quasiperiodic oscillations split into two curves, one for an Andronov-Hopf bifurcation and another one for a Neimark-Sacker bifurcation.

If Δ_γ is sufficiently large, multistability in (6) emerges. In Fig. 8(c), we show the two-dimensional bifurcation diagram on the parametric plane (p, γ) . Just as in case of the reduced system (5) (see Fig. 3(c)), the tip of the synchronization tongue has an increased width. Such bifurcational structure has appeared due to the emergence of two new curves for saddle-node bifurcations: L_{SN_1} and L_{SN_2} (see Fig. 8(d)). Therefore, after two saddle-node bifurcations, there are two stable limit cycles laying on the same two-dimensional ergodic torus that appears with a pair of two saddle limit cycles which separate one stable cycle from the other.

The appearance of coexisting limit cycles as the result of saddle-node bifurcations is illustrated in Fig. 11(a). It should be noted that the limit cycles $C_{1,2}$ and $C'_{1,2}$ are situated on the surface of a two-dimensional torus (see Fig. 11(b)). Therefore, the disappearance of a couple of limit cycles as the result of a saddle-node bifurcation (SN_2 or SN_1)

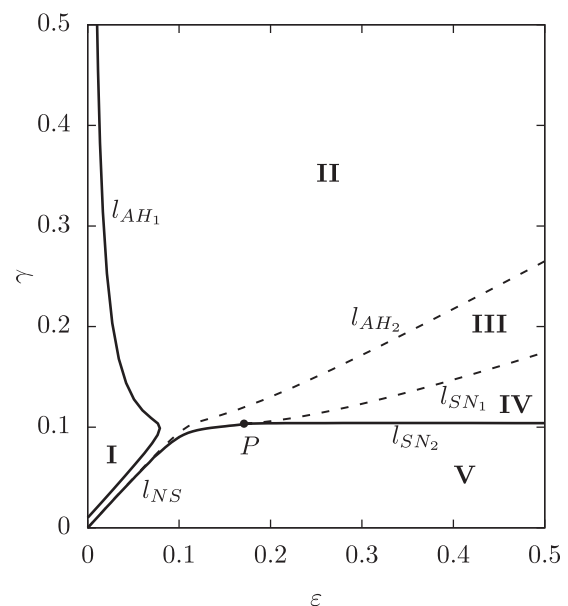


FIG. 10. Two-parametric bifurcation diagram for system (6) on the parametric plane (ε, γ) for $p = 1.1$, $\Delta_\gamma = -0.01$. Here, $l_{AH_{1,2}}$ are the curves for Andronov-Hopf bifurcations.

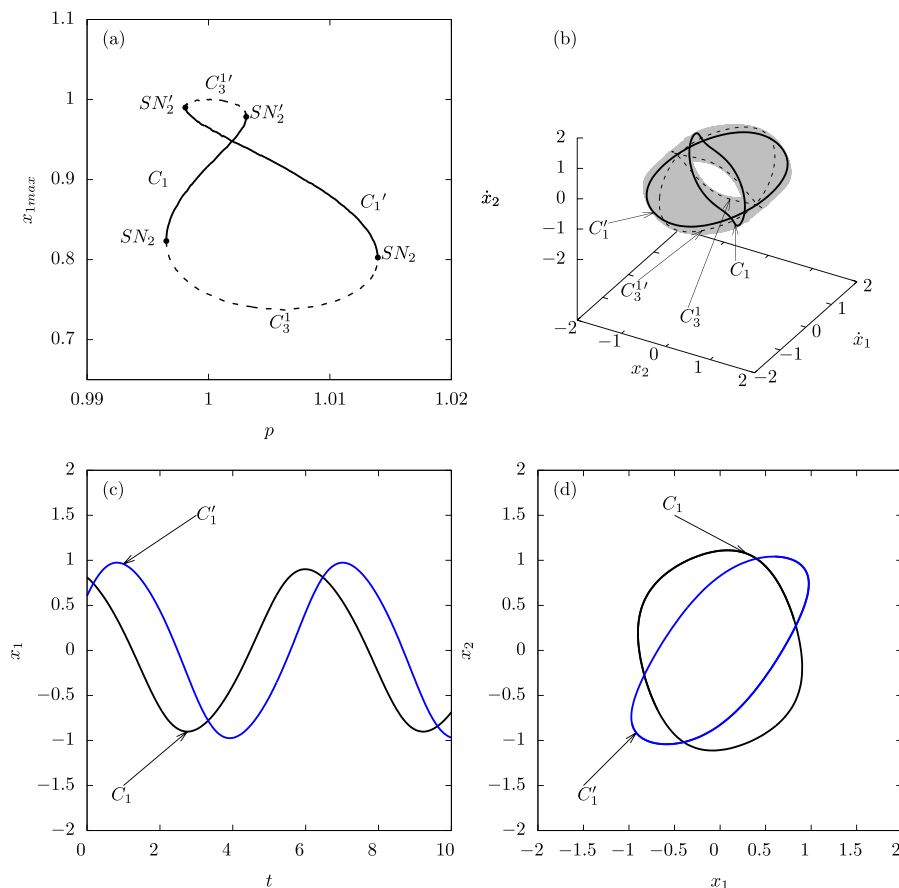


FIG. 11. (a) Emergence of coexisting stable limit cycles in (6) when crossing the synchronization region at $\gamma = 0.044$. (b) Phase portrait of system (6) with $\varepsilon = 0.25$, $p = 0.999$, $\gamma = 0.044$. Here, C_1 and C_1' are the stable limit cycles, C_3 and C_3' are the saddle limit cycles. (c) Time series of the coexisting stable limit cycles. (d) Projections of the coexisting stable limit cycles on the plane (x_1, x_2) .

does not lead to the emergence of a stable torus, and the phase point goes to the residual stable limit cycle on the torus. Hence, the bifurcational scenario of appearance of bistability and the corresponding bifurcational structure of the parameter space obtained from the reduced model (5) completely describes the bifurcational mechanisms underlying the synchronization and multistability in the initial model of two asymmetrically coupled van der Pol oscillators. The phases of the coexisting limit cycles C_1 , C_1' are shifted on the quarter of period, which can be seen from panel (c) of Figure 11. At the same time, their periods are close: the period of oscillations corresponding to limit cycle C_1 is 6.473, while for C_1' the period is 6.196.

IV. CONCLUSIONS

In this paper, we have studied a system of two van der Pol oscillators characterized by asymmetry in dissipative coupling. The dynamics of this system has been considered in a quasi-harmonic approach as well as without any reduction.

We have found that the introduction of small asymmetry affects the structure of synchronization region in the parameter space in the same way as the introduction of non-identity in nonlinearity parameters of interacting oscillators. As the result of asymmetry in interaction, a “wideband synchronization channel”³⁵ emerges. Increase of asymmetry and transition to repulsive interaction leads even to the formation of multistability in the phase space of the system: two stable limit cycles coexist on the surface of a two-dimensional torus. It also should be emphasized that the bifurcation structure of the synchronization region in the parameter space undergoes

significant changes. The tip of the Arnold’s tongue widens due to the formation of folds defined by saddle-node bifurcation curves for the limit cycles on the torus.

It also should be noted that the considered model is described by a four-dimensional dissipative nonlinear dynamical system. Therefore, there is a possibility to obtain a chaotic attractor in its phase space. However, our main goal was to consider the regular dynamics for relatively small nonlinearity and coupling coefficient values, and therefore we did not carry out an analysis for the emergence of a chaotic attractor. In particular, we cannot exclude the possibility for a chaotic behavior of the model in a wider area of the parameter space, this will be the subject for further research.

The presented results are of special importance for the studies of different basic biological systems, e.g., neural ensembles as they are modeled by networks of van der Pol oscillators or even their phase reduction—Kuramoto oscillators.³⁷ It should be emphasized that the bistability phenomenon observed above is realized for a weak coupling between oscillators. Taking into account that it was experimentally verified in Ref. 38 that the interaction between neurons is weak, our results are relevant to neuroscience and can be used to describe the phenomena of multistability and cluster synchronization in neural ensembles of different size and topology.

ACKNOWLEDGMENTS

S.A. was supported by RFBR, Research Project No. 16-37-00104. N.F. was supported by CREST, JST. J.K. was supported by the IRTG 1740/TRP 2011/50151-0.

- ¹A. Pikovsky, M. Rosenblum, and J. Kurths, *Synchronization: A Universal Concept in Nonlinear Science* (Cambridge University Press, Cambridge, 2003).
- ²V. Anishchenko, V. Astakhov, A. Neiman, T. Vadivasova, and L. Shimansky-Geier, *Nonlinear Dynamics of Chaotic and Stochastic Systems. Tutorial and Modern Development* (Springer, Berlin, 2007).
- ³K. P. O’Keeffe, P. L. Krapivsky, and S. H. Strogatz, “Synchronization as aggregation: Cluster kinetics of pulse-coupled oscillators,” *Phys. Rev. Lett.* **115**, 064101 (2015).
- ⁴P. Kumar, D. K. Verma, P. Parmananda, and S. Boccaletti, “Experimental evidence of explosive synchronization in mercury beating-heart oscillators,” *Phys. Rev. E* **91**, 062909 (2015).
- ⁵M. R. Showalter and D. P. Hamilton, “Resonant interactions and chaotic rotation of Pluto’s small moons,” *Nature* **522**, 45–49 (2015).
- ⁶T. Banerjee, P. S. Dutta, and A. Gupta, “Mean-field dispersion-induced spatial synchrony, oscillation and amplitude death, and temporal stability in an ecological model,” *Phys. Rev. E* **91**, 052919 (2015).
- ⁷Z. B. Guo and P. H. Diamond, “From phase locking to phase slips: A mechanism for a quiescent h mode,” *Phys. Rev. Lett.* **114**, 145002 (2015).
- ⁸Z. P. Kilpatrick, “Stochastic synchronization of neural activity waves,” *Phys. Rev. E* **91**, 040701 (2015).
- ⁹C.-J. Jin, W. Wang, R. Jiang, H. M. Zhang, and H. Wang, “Spontaneous phase transition from free flow to synchronized flow in traffic on a single-lane highway,” *Phys. Rev. E* **87**, 012815 (2013).
- ¹⁰C. Huygens, *Horologium oscillatorium: sive, De motu pendulorum ad hologia aptato demonstrationes geometricae* (F. Muguet, 1673).
- ¹¹T. Tanaka and T. Aoyagi, “Multistable attractors in a network of phase oscillators with three-body interactions,” *Phys. Rev. Lett.* **106**, 224101 (2011).
- ¹²V. Anishchenko, S. Astakhov, and T. Vadivasova, “Phase dynamics of two coupled oscillators under external periodic force,” *Europhys. Lett.* **86**, 30003 (2009).
- ¹³E. M. Izhikevich, “Weakly connected quasi-periodic oscillators, FM interactions, and multiplexing in the brain,” *SIAM J. Appl. Math.* **59**, 2193–2223 (1999).
- ¹⁴M. G. Rosenblum, A. S. Pikovsky, and J. Kurths, “Phase synchronization of chaotic oscillators,” *Phys. Rev. Lett.* **76**, 1804–1807 (1996).
- ¹⁵V. Anishchenko, T. Vadivasova, D. Postnov, and M. Safonova, “Synchronization of chaos,” *Int. J. Bifurcation Chaos* **2**, 633–644 (1992).
- ¹⁶L. M. Pecora and T. L. Carroll, “Synchronization in chaotic systems,” *Phys. Rev. Lett.* **64**, 821–824 (1990).
- ¹⁷H. Fujisaka and T. Yamada, “Stability theory of synchronized motion in coupled-oscillator systems,” *Prog. Theor. Phys.* **69**, 32–47 (1983).
- ¹⁸S. Astakhov, A. Feoktistov, V. S. Anishchenko, and J. Kurths, “Synchronization of multi-frequency noise-induced oscillations,” *Chaos* **21**, 047513 (2011).
- ¹⁹A. Neiman, X. Pei, D. Russell, W. Wojtenek, L. Wilkens, F. Moss, H. A. Braun, M. T. Huber, and K. Voigt, “Synchronization of the noisy electro-sensitive cells in the paddlefish,” *Phys. Rev. Lett.* **82**, 660–663 (1999).
- ²⁰B. V. der Pol, “On relaxation-oscillations,” *London, Edinburgh Dublin Philos. Mag. J. Sci.* **2**, 978–992 (1927).
- ²¹M. Barrón and M. Sen, “Synchronization of four coupled van der Pol oscillators,” *Nonlinear Dyn.* **56**, 357–367 (2009).
- ²²G. Osipov, J. Kurths, and C. Zhou, *Synchronization in Oscillatory Networks*, Springer Series in Synergetics (Springer, 2007).
- ²³D. Aronson, G. Ermentrout, and N. Kopell, “Amplitude response of coupled oscillators,” *Physica D* **41**, 403–449 (1990).
- ²⁴B. Sonnenschein, T. K. D. Peron, F. A. Rodrigues, J. Kurths, and L. Shimansky-Geier, “Collective dynamics in two populations of noisy oscillators with asymmetric interactions,” *Phys. Rev. E* **91**, 062910 (2015).
- ²⁵Z. Levnajić, “Emergent multistability and frustration in phase-repulsive networks of oscillators,” *Phys. Rev. E* **84**, 016231 (2011).
- ²⁶I. Belykh, R. Reimbayev, and K. Zhao, “Synergistic effect of repulsive inhibition in synchronization of excitatory networks,” *Phys. Rev. E* **91**, 062919 (2015).
- ²⁷Z. Levnajić and B. Tadić, “Stability and chaos in coupled two-dimensional maps on gene regulatory network of bacterium *E. coli*,” *Chaos* **20**, 033115 (2010).
- ²⁸M. I. Rabinovich, P. Varona, A. I. Selverston, and H. D. I. Abarbanel, “Dynamical principles in neuroscience,” *Rev. Mod. Phys.* **78**, 1213–1265 (2006).
- ²⁹P.-J. Kim, T.-W. Ko, H. Jeong, and H.-T. Moon, “Pattern formation in a two-dimensional array of oscillators with phase-shifted coupling,” *Phys. Rev. E* **70**, 065201 (2004).
- ³⁰I. Leyva, I. Sendiña Nadal, J. A. Almendral, and M. A. F. Sanjuán, “Sparse repulsive coupling enhances synchronization in complex networks,” *Phys. Rev. E* **74**, 056112 (2006).
- ³¹I. Leyva, E. Allaria, S. Boccaletti, and F. T. Arecchi, “In phase and anti-phase synchronization of coupled homoclinic chaotic oscillators,” *Chaos* **14**, 118–122 (2004).
- ³²S. Astakhov, N. Fujiwara, A. Gulay, N. Tsukamoto, and J. Kurths, “Hopf bifurcation and multistability in a system of phase oscillators,” *Phys. Rev. E* **88**, 032908 (2013).
- ³³K. Premalatha, V. K. Chandrasekar, M. Senthilvelan, and M. Lakshmanan, “Impact of symmetry breaking in networks of globally coupled oscillators,” *Phys. Rev. E* **91**, 052915 (2015).
- ³⁴N. Bogoliubov and Y. Mitropolski, *Asymptotic Methods in the Theory of Non-Linear Oscillations* (Gordon and Breach, New York, 1961).
- ³⁵A. Kuznetsov and J. Roman, “Synchronization of coupled anisochronous auto-oscillating systems,” *Nonlinear Phenom. Complex Syst.* **12**, 54–60 (2009).
- ³⁶V. Astakhov, S. Koblyanskii, A. Shabunin, and T. Kapitaniak, “Peculiarities of the transitions to synchronization in coupled systems with amplitude death,” *Chaos* **21**, 023127 (2011).
- ³⁷Z. Levnajić and A. Pikovsky, “Phase resetting of collective rhythm in ensembles of oscillators,” *Phys. Rev. E* **82**, 056202 (2010).
- ³⁸A. J. Preyer and R. J. Butera, “Neuronal oscillators in *Aplysia californica* that demonstrate weak coupling *In Vitro*,” *Phys. Rev. Lett.* **95**, 138103 (2005).